



DAPNIA/SPP 96-01

January 1996

SELECTED RESULTS FROM THE DØ EXPERIMENT

A. Zylberstejn

*Presented at the ITEP Conference on
"Fundamental Interactions of Elementary Particles",
Moscow, 22-29 October 1995*

DAPNIA

Le DAPNIA (**D**épartement d'**A**strophysique, de physique des Particles, de physique Nucléaire et de l'**I**nstrumentation Associée) regroupe les activités du Service d'Astrophysique (SAp), du Département de Physique des Particles Elémentaires (DPhPE) et du Department de Physique Nucléaire (DPhN).

Adresse : DAPNIA, Bâtiment 141
 CEA Saclay
 F -91191 Gif-sur-Yvette Cedex

Selected results from the DØ Experiment ¹

A. Zylberstejn (DAPNIA/SPP C.E. Saclay, France)

For the DØ Collaboration

Abstract

In this paper we review some of the recent results obtained with the DØ detector as they were available at the end of the Summer of 1995. The data have been accumulated during 2 collider runs between May 1992 and July 1995. During the first run (run 1A) and second run (Run 1B) total luminosities of 14 pb^{-1} and 85 pb^{-1} respectively have been accumulated. For most of the results presented here only data from run 1A have been used.

1 Introduction

DØ is a large multi-purpose detector operating at the Tevatron $\bar{p}p$ Collider, located at Fermi National Accelerator Laboratory. The DØ collaboration consists of approximately 430 physicists from 44 institutions in 9 countries. The research program encompasses a wide variety of basic phenomena. The program can be divided into five major areas – top physics, W and Z physics, new particle searches, studies of the strong interaction QCD and b -quark studies (see ref. [1] to [24]).

2 The DØ detector

The DØ detector [1] features three major subsystems: central tracking detectors (with no central magnetic field), nearly hermetic liquid argon calorimetry, and a muon spectrometer.

The central tracking system, consisting of drift chambers and a transition radiation detector (TRD), is used to identify charged tracks in the pseudorapidity range $|\eta| \leq 3.5$. Its small outer radius helps to reduce the backgrounds to muons from π and K decays. The tracking chambers serve to establish the primary event vertex and confirm candidate lepton tracks. The dE/dx measurements in the drift chambers and the signals from the TRD allow extra rejection of background to electrons.

The liquid argon calorimeters provide full angular coverage for $|\eta| \leq 4.2$. They permit good multijet discrimination with relatively small corrections to the observed jet energies. Discrimination of electrons and pions is given by the pattern of energy deposits in the calorimeter.

Good E_T resolution is achieved for signalling the presence of neutrinos, due to the good energy resolution and hermetic calorimeter coverage. From test beam studies, energy resolution is approximately $15\%/\sqrt{E}$ for electrons and approximately $50\%/\sqrt{E}$ for hadrons.

The muon detector is sensitive over the interval $|\eta| < 3.3$. It consists of proportional drift tube chambers before and after magnetized iron toroids surrounding the calorimeters. The magnetic field in the iron toroids provides a momentum measurement with a resolution $\delta p/p = [(\frac{0.18(p-2)}{p})^2 + (0.008p)^2]^{1/2}$, (p in GeV/ c). The large amount of material in the calorimeters and toroids (between 13 and 18 absorption lengths) suppresses backgrounds due to the leakage of hadronic showers.

¹Presented at the ITEP Conference on "Fundamental Interactions of Elementary Particles" (Moscow, Oct. 1995)

3 Particles identification

3.1 Electrons

Electrons are identified by their longitudinal and transverse shower profile in the calorimeter and are required to have a matching track in the central tracking chambers. The background from photon conversions is suppressed by an ionization (dE/dx) criterion on the chamber track. The TRD is used to confirm the identity of electrons for $|\eta| < 1$.

The electron energy scale is set using the mass of Z boson. The linearity of the calibration is checked making use of the range of electron energies from Z decays, and the π^0 (from $\pi^0 \rightarrow \gamma\gamma$ in which both photons produce electrons from photoconversion) and $J/\Psi \rightarrow e^+e^-$ peaks. The relative uncertainty on the electron energy scale is 0.5% .

3.2 Jets

Jets are found with the calorimeter only, using a fixed cone algorithm in η, ϕ space . The radius of the cone is adapted to the reaction under study. For instance in the top analysis, $\mathcal{R} = 0.5$ is used.

The jet energy scale is set by requiring E_T balance in events with a normal (hadronic) jet and a predominantly electromagnetic jet or photon. The relative uncertainty in the jet energy scale is 10%. The jets are also required to pass loose shape cuts to remove events with extra energy due to electronic noise or accelerator backgrounds

3.3 Muons

The thickness of the calorimeter plus iron toroids varies from 14 λ in the central region to 19 λ in the forward region. This reduces the hadronic punchthrough background to a negligible level ($< 0.5\%$) and allows a good identification of muons in jets. Muon candidates are confirmed by their ionization in the calorimeter.

3.4 Neutrinos

The presence of neutrinos in the final state is inferred from missing transverse energy (\cancel{E}_T). The calorimeter-only \cancel{E}_T ($\cancel{E}_T^{\text{cal}}$) is determined from energy deposition in the calorimeter for $|\eta| < 4.5$. The total \cancel{E}_T is determined by correcting $\cancel{E}_T^{\text{cal}}$ for the measured p_T of detected muons.

4 Top Quark Physics

The top quark is the sixth and final quark required by the Standard Model particle theory. (Other quarks may exist, but they would be by definition “non-standard.”) The search for and study of the Standard Model top quark has been and remains an extremely active area of research in $D\bar{O}$. The increasing luminosity delivered by the Fermilab Tevatron has permitted the search to be carried out with ever greater sensitivity. Since the beginning of 1994, $D\bar{O}$ has published three papers on the search for the top quark. [4][6] The last of these [7] , which was submitted simultaneously with a similar paper by CDF, [28], represents the successful culmination of a long effort to find the top

quark. With this observation the discovery phase is over, and we can start to study the properties of the top quark.

The top quark search in $D\bar{D}$ assumes that the top quark is produced in pairs by the strong interaction, and decays 100% of the time into a W boson and a b quark, as required by the Standard Model. Top quark events are divided into different categories depending on how the W bosons decay. The main searches take place in modes where both W 's decay into leptons (the dilepton modes: $e\mu$, ee , and $\mu\mu$) or where just one W decays leptonically (the single-lepton modes: e and μ). The single-lepton modes are further categorized on the basis of soft-muon-tagging of the b quarks or "topological" event selection. In addition to the dilepton and single-lepton modes, the top quark pair may decay into τ leptons (with at least one τ decaying into hadrons) or only into quarks. In all modes, final state quarks are observed as jets and neutrinos are observed as missing transverse energy.

The main areas of research in top quark physics in $D\bar{D}$ are as follows [4],[6],[7],[14] :

- Conventional searches in the dilepton and single-lepton modes.
- Mass analysis in the dilepton and single-lepton modes.
- Multivariate searches in the dilepton and single-lepton modes.
- Searches for top decays involving hadronically decaying τ 's.
- Search for top in the all-quark (also called all-jets) decay mode.
- Search for top quarks produced singly by the weak interaction.

So far, most of the published and presented results have been in the area of the first two items in this list. However, groups in $D\bar{D}$ are working on all of the above topics.

4.1 The Conventional Counting Experiment

The data set for this analysis includes data from run 1A and run 1B with an integrated luminosity of about 50pb^{-1} , with slight differences among the seven channels. The event selection is chosen to give maximum expected significance for top quark masses of 180–200 GeV/c^2 , using the ISAJET event generator [33] to model the top quark signal (assuming the Standard Model top quark pair production cross section of Ref. [29]), and using our standard background estimates as described below. We achieve a signal-to-background ratio of 1:1 for a top quark mass of 200 GeV/c^2 . This is a better signal-to-background ratio, but with smaller acceptance, than our previously published analyses [4, 6].

The improved rejection arises primarily by requiring events to have a larger total transverse energy by means of a cut on a quantity H_T , defined as the scalar sum of the E_T 's of the jets (for the single-lepton and $\mu\mu + \text{jets}$ channels), or the scalar sum of the E_T 's of the leading electron and the jets (for the $e\mu + \text{jets}$ and $ee + \text{jets}$ channels). The power of a selection using H_T is illustrated in Figure 1 which shows a comparison of the shapes of the H_T distributions expected from background and 200 GeV/c^2 top quarks in the channels (a) $e\mu + \text{jets}$ and (b) untagged single-lepton + jets.

In the conventional top quark search, one attempts to isolate a nearly pure sample of top quark events by means of one- and two-dimensional cuts on a limited number of variables.

Table 1: Minimum kinematic requirements for the standard event selection (energy in GeV).

Channel	High- p_T Leptons		Jets		Missing E_T		Muon Tag	Topological	
	$E_T(e)$	$p_T(\mu)$	N_{jet}	$E_T(\text{jet})$	$\cancel{E}_T^{\text{cal}}$	\cancel{E}_T	$p_T(\mu)$	H_T	\mathcal{A}
$e\mu + \text{jets}$	15	12	2	15	20	10	-	120	-
$ee + \text{jets}$	20		2	15	25	-	-	120	-
$\mu\mu + \text{jets}$		15	2	15	-	-	-	100	-
$e + \text{jets}$	20		4	15	25	-	-	200	0.05
$\mu + \text{jets}$		15	4	15	20	20	-	200	0.05
$e + \text{jets}/\mu$	20		3	20	20	-	4	140	-
$\mu + \text{jets}/\mu$		15	3	20	20	20	4	140	-

The signature for the dilepton channels is defined as two isolated leptons, two or more jets, and large \cancel{E}_T . The signature for the single-lepton channels is defined as one isolated lepton, large \cancel{E}_T , and three or more jets (with muon tag) or four or more jets (without tag). The single-lepton signature includes either a soft muon tag or a “topological tag” based on H_T and the aplanarity of the jets \mathcal{A} . The aplanarity is proportional to the smallest eigenvalue of the momentum tensor of the jets in the laboratory [34] and ranges from 0–0.5. “Double-tagged” events are counted only once, as part of the muon tagged channels.

Electrons are required to have $|\eta| < 2.5$ and transverse energy $E_T > 15$ GeV. Two distinct types of muons are defined. “High- p_T ” muons, which are predominantly from gauge boson decay, are required to be isolated from jet axes by distance $\Delta\mathcal{R} > 0.5$ in η - ϕ space ($\eta = \text{pseudorapidity} = \tanh^{-1}(\cos \theta)$; $\theta, \phi = \text{polar, azimuthal angle}$), and to have transverse momentum $p_T > 12$ GeV/ c . “Soft” muons, which are primarily from b, c or π/K decay, are required to be within distance $\Delta\mathcal{R} < 0.5$ of any jet axis. The minimum p_T for soft muons is 4 GeV/ c . The maximum η for both kinds of muons is 1.7 for run Ia data and 1.0 for run Ib data. The maximum muon η is determined by the edge of the wide angle muon spectrometer. The η restriction is tightened for some run Ib data due to forward muon chamber aging. Jets are reconstructed using a cone algorithm of radius $\mathcal{R} = 0.5$. A summary of the kinematic cuts can be found in Table 1.

Additional special cuts are used in the $ee + \text{jets}$, $\mu\mu + \text{jets}$, and $\mu + \text{jets}/\mu$ channels to remove background from $Z + \text{jets}$. To remove $Z \rightarrow ee$ background in $ee + \text{jets}$, we require that $|m_{ee} - m_Z| > 12$ GeV/ c^2 or $\cancel{E}_T^{\text{cal}} > 40$ GeV. Because of $D\phi$ ’s coarse muon momentum resolution, which is limited by multiple scattering to about 20%, a dimuon invariant mass cut does not effectively remove background from $Z \rightarrow \mu\mu$ with reasonable efficiency. To remove this background, we require that the event as a whole is inconsistent with the $Z + \text{jets}$ hypothesis based on a global kinematic fit. The loose event selection cuts differ from those listed in Table 1 by the removal of the H_T requirement and by the relaxation of the aplanarity requirement for $e + \text{jets}$ and $\mu + \text{jets}$ from $\mathcal{A} > 0.05$ to $\mathcal{A} > 0.03$.

The acceptance for $t\bar{t}$ events is calculated using the ISAJET event generator and a detector simulation based on the GEANT program [36]. As a check, the acceptance is also calculated using the HERWIG event generator [37]. The difference between ISAJET and HERWIG is included in the systematic error.

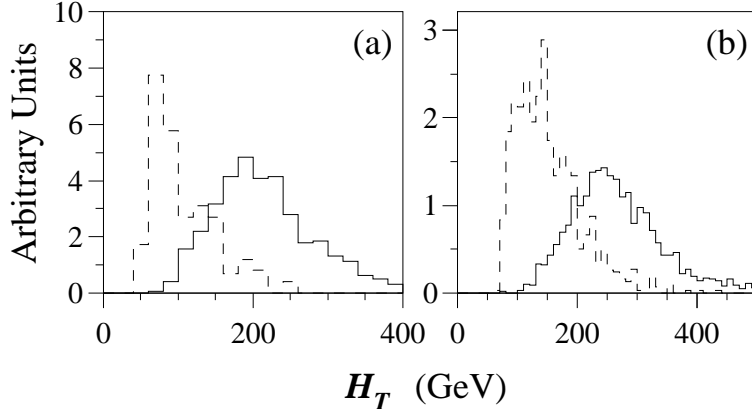


Figure 1: Shape of H_T distributions expected for the principal backgrounds (dashed line) and $200 \text{ GeV}/c^2$ top quarks (solid line) for (a) $e\mu + \text{jets}$ and (b) untagged single-lepton + jets.

Physics backgrounds (those having the same final state particles as the signal) are estimated using Monte Carlo simulation, or a combination of Monte Carlo and data. The instrumental background from jets misidentified as electrons is estimated entirely from data using the measured jet misidentification probability (typically 2×10^{-4}). Other backgrounds for muons (*e.g.* hadronic punchthrough and cosmic rays) are negligible for the signatures in question.

For the dilepton channels, the principle backgrounds are from Z and continuum Drell-Yan production ($Z, \gamma^* \rightarrow ee, \mu\mu$, and $\tau\tau$), vector boson pairs (WW, WZ), heavy flavor ($b\bar{b}$ and $c\bar{c}$) production, and backgrounds with jets misidentified as leptons.

For the untagged single-lepton channels, the principle backgrounds are from $W + \text{jets}$, $Z + \text{jets}$, and QCD multijet production with a jet misidentified as a lepton. The $W + \text{jets}$ background is estimated using jet-scaling. In this method, we extrapolate the $W + \text{jets}$ cross section from one and two jets, to four or more jets assuming an exponential dependence on the number of jets, as predicted by QCD [35], and as observed experimentally. The efficiency of the topological cuts for $W + 4$ jets is calculated using the VECBOS Monte Carlo program [35]. The QCD multijet background is determined independently from data using the measured jet fake probability. The $Z + \text{jets}$ background is estimated by Monte Carlo calculation.

For the tagged single-lepton channels, the observed jet multiplicity spectrum of untagged background events is convoluted with the measured tagging rate per jet to determine the total background. The tagging rate is observed to be a function of the number of jets in the event and the E_T of the jets and is the same within error for both multijet and $W + \text{jets}$ events. As a cross check, tagging-rate predictions are made for dijet, multijet, and gamma+jet samples and found to agree with the data.

From all seven channels, we with the standard event selection we observe 17 events with an expected background of 3.8 ± 0.6 events (see Table 2). Our measured cross section as a function of the top quark mass hypothesis is shown in Fig. 2. Assuming a top quark mass of $200 \text{ GeV}/c^2$, the production cross section is $6.3 \pm 2.2 \text{ pb}$. The error in the cross section includes an overall 12% uncertainty in the luminosity. The probability of an upward fluctuation of the background to 17 or more events is 2×10^{-6} , which corresponds to 4.6 standard deviations for a Gaussian

Table 2: $D\bar{O}$ counting experiment summary for all channels for $\int \mathcal{L} dt \approx 50 pb^{-1}$, .

	Standard Selection	Loose Selection
Dileptons	3	4
Lepton + Jets (Topological)	8	23
Lepton + Jets (Muon tag)	6	6
All channels	17	33
Background	3.8 ± 0.6	20.6 ± 3.2
Probability	$2 \times 10^{-6} (4.6\sigma)$	$0.023 (2.0\sigma)$
$\sigma_{t\bar{t}} (m_t = 200 \text{ GeV}/c^2)$	$6.3 \pm 2.2 \text{ pb}$	$4.5 \pm 2.5 \text{ pb}$

probability distribution. The excess is distributed across all of the channels in a manner consistent with Standard Model top quark decay branching ratios. We conclude that we have observed the top quark.

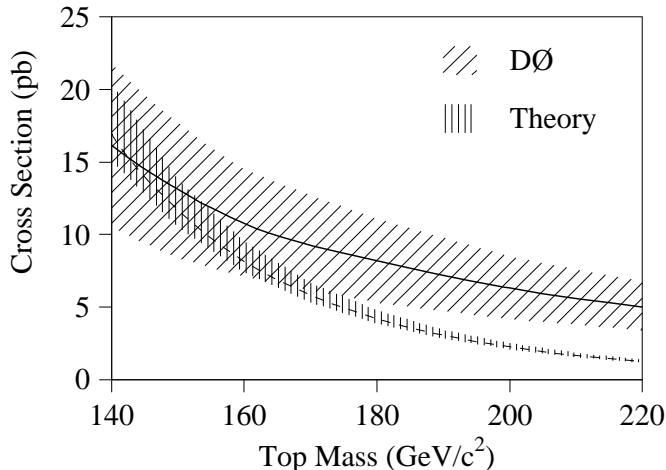


Figure 2: $D\bar{O}$ measured $t\bar{t}$ production cross section (solid line with one standard deviation error band) as a function of assumed top quark mass. Also shown is the theoretical cross section curve (dashed line) [29].

4.2 Mass Analysis

The goal of the mass analysis is the direct measurement of the top quark mass. It is possible to perform mass analyses in either the dilepton or single-lepton decay modes.

4.2.1 Singl-lepton + jets

The mass analysis of $t\bar{t} \rightarrow l\nu q\bar{q}'b\bar{b}$ candidate events effectively uses six measured vectors: the lepton momentum, the \cancel{E}_T , and the momenta of four jets as approximations to the true momenta of the lepton, neutrino and four quarks in each event. These, along with resolution functions and background shapes, are input to a two-constraint(2C) kinematic fit. The constraints include overall momentum conservation, equality of the reconstructed masses of both top quarks, and the difference between the mass of the reconstructed W 's and the W mass. Events with at least 4 jets have been used for this analysis. The fits were performed on all permutations of the jet assignments of the four highest E_t jets (using a $\mathcal{R} = 0.3$ cone algorithm). The muon-tagged jets were assigned to a b quark.

Up to 3 permutations with $\chi^2 < 7$ (2 degrees of freedom) were retained and a single χ^2 - probability-weighted average mass was calculated for each event. Effects of gluon radiation, jet assignment combinatorics, and the event selection procedure result in a mass-dependent shift between the fitted mass and the true top which was taken into account in the final mass determination.

Eleven of the 14 lepton+jets events selected using the standard cuts and 24 of the 27 events with the loose cuts, were fitted successfully. An unbinned likelihood fit, incorporating top quark and background contribution was performed on the fitted mass distributions. This gives a top quark mass of 199_{-25}^{+31} GeV/ c^2 for the standard cuts and 199_{-21}^{+19} GeV/ c^2 for the loose cuts.

The systematic error on the mass determination is dominated by the jet energy scale uncertainty which is estimated to be $< 10\%$. This corresponds to an error in the final result of $_{-20}^{+12}$ GeV/ c^2 (using ISAJET).

Other sources of systematic errors include:

- Event generator (using Herwig instead of Isajet): ≈ 4 GeV/ c^2 .
- Fitting method: ≈ 4 GeV/ c^2 .
- Determination of QCD fraction: ≈ 2 GeV/ c^2 .
- Other systematic effects: < 5 GeV/ c^2 .

Removing the background constraint for the loose sample changes the result by less than 1 GeV/ c^2 , with the error increasing by about 10%. The total systematic error on the mass determination is: $_{-21}^{+14}$ GeV/ c^2

Our result for the top mass is:

$$\begin{aligned} m_t &= 199_{-21}^{+19}(\text{stat.})_{-21}^{+14}(\text{syst.}) \text{ GeV}/c^2 \\ &= 199_{-30}^{+24} \text{ GeV}/c^2 . \end{aligned}$$

Figure 3 shows the top quark mass distribution of fully reconstructed candidate top quark events for two sets of event selection cuts.

4.2.2 Dilepton Mass Analysis

In addition to the lepton + jet channels, the events in the dilepton channels also contain mass information. The following describes a preliminary mass analysis in the dilepton channels based on ideas of Dalitz and Goldstein [25] and Kondo [26].

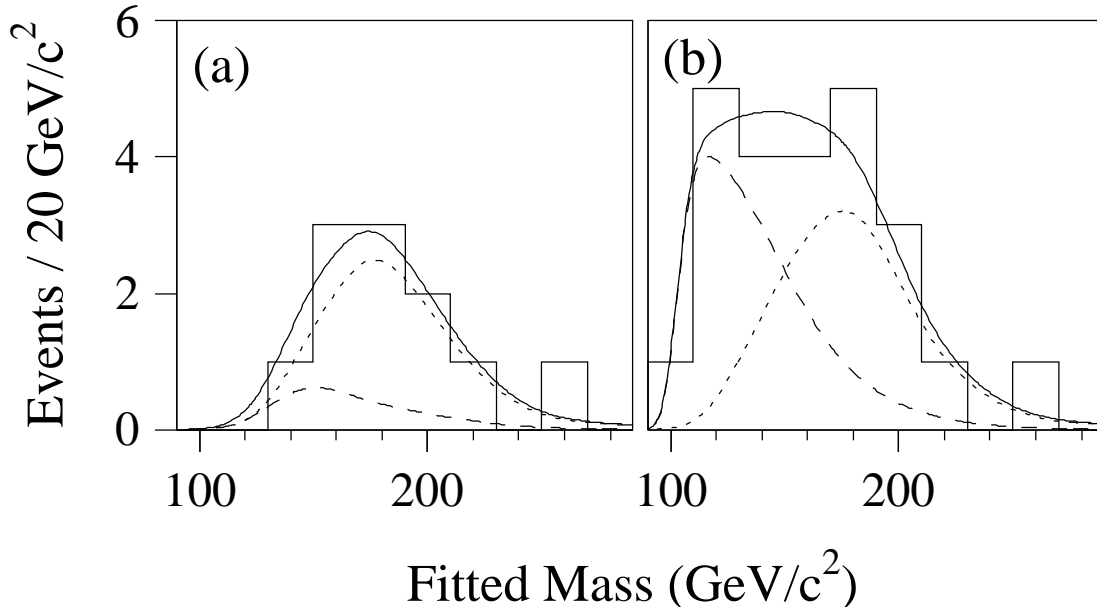


Figure 3: Fitted mass distribution for candidate events (histogram) with the expected mass distribution for $199 \text{ GeV}/c^2$ top quark events (dotted curve), background (dashed curve), and the sum of top and background (solid curve) for (a) standard and (b) loose event selection.

The sample, corresponding to $\int \mathcal{L} dt \approx 72 \text{ pb}^{-1}$, contains five dilepton candidates (1 ee , 2 $e\mu$, and 2 $\mu\mu$) with an estimated background of about 1 event

Once the top mass is specified, the kinematics of a dilepton event can be completely specified up to a possible 4-fold ambiguity in the neutrino solutions. However, not all solutions are equally likely. Each solution is weighted by

$$\mathcal{A}(m_t) f(x) f(\bar{x}) p(E^*(l)|m_t) p(E^*(\bar{l})|m_t), \quad (1)$$

where $f(x)$ is the parton distribution for the valence quarks, $p(E^*(l)|m_t)$ is the probability distribution for the energy of the charged lepton in the top rest frame, and $\mathcal{A}(m_t)$ is a normalization factor chosen so that the average of the weights over $t\bar{t}$ phase space is constant with respect to m_t . This gives a likelihood curve as a function of m_t . To account for detector resolution, the event is smeared many times with appropriate resolutions. The position of the peak of the likelihood distribution, m_{peak} , is used as an estimate of the top mass. To extract a measurement of the top quark mass from our sample of dilepton events we perform a maximum likelihood fit to the distribution of the observed mass.

The statistical error, estimated using the width of the ensemble fit distribution, is $\sim 25 \text{ GeV}/c^2$ for a mass $\sim 145 \text{ GeV}/c^2$. The estimated systematic error is $\sim 20 \text{ GeV}/c^2$, with the dominant contributions coming from the jet energy scale and the dependence on the Monte Carlo generator used. Other contributions include errors for signal resolution function determination, background parameterization, and choice of weight functions.

The preliminary mass result from the dilepton channels is

$$m_t(\text{dilepton}) \sim 145 \pm 25(\text{stat.}) \pm 20(\text{syst.}) \text{ GeV}/c^2 . \quad (2)$$

Using only the two $e\mu$ events yields nearly the same result as the full 5 event sample.

4.3 Multivariate Analyses

Multivariate techniques are an alternative to the conventional cuts method of isolating a nearly pure sample of top quark events. In conventional analyses, one is in practice limited to making one- and two-dimensional cuts. In multivariate analysis, various techniques are used to generate multi-dimensional cuts for optimal separation of signal and background. Three techniques are currently being studied in $D\emptyset$: Neural networks, probability density estimation (PDE), and the ‘‘H-matrix’’ (or covariance matrix) technique.

In all cases, the goal of the multivariate analysis methods is to improve the signal to background ratio over that which can be obtained using conventional analysis for a given efficiency. Since the top quark statistics will be limited for the foreseeable future, multivariate techniques may produce the largest possible sample of top quark events for mass analysis or for other studies. Multivariate techniques may also aid in isolating signals in the more difficult decay modes described in the next section.

In the single lepton+jets mode the product of efficiency and branching ratio is 3.1% using the PDE analysis and 4.0% using the neural network analysis, compared to 1.8% for conventional analysis for 180 GeV/c^2 top mass. In both analyses the measured $t\bar{t}$ cross-section is in agreement with the results of the conventional analysis.

4.4 Other Decay Modes

The top decay modes involving τ leptons and the all-quark decay modes are more difficult than the dilepton and single-lepton decay modes due to larger backgrounds. Results on these modes have not yet been published by $D\emptyset$. However, the Standard Model makes definite predictions on the branching ratios of these decay modes relative to the dilepton and single-lepton decay modes. The measurement of the τ and all-quark decay modes are important for confirming that the massive particle signals observed by $D\emptyset$ are in fact the Standard Model top quark. For example, one way in which the top quark may be non-standard is if it decays some of the time into a charged Higgs boson H^\pm instead of a W boson. Unlike the W boson, the charged Higgs decays predominantly into τ leptons rather than e or μ leptons. Therefore, excess τ decays could be evidence for charged Higgs being produced by top decay.

The all-quark decay mode has the largest branching ratio of all of the decay modes. It is the only neutrinoless decay mode which makes it potentially useful for mass analysis. Preliminary results show evidence of a small excess of observed events over estimated background.

4.5 Single Top Quark Production

In addition to the dominant strong interaction pair production mechanism, top quarks may be produced singly by the weak interaction. Relative to the amount of phase space available, single top production is much weaker than pair production, and the backgrounds are therefore worse. However, single-top events would be very interesting if they could be isolated. The production mechanisms for single top production provide an interesting test of the Standard Model in their own right. The mass analysis of single-top quark events is much more straightforward than the mass analysis of top quark pair events. Another interesting feature of singly produced top quarks is that they are produced polarized, which permits measurements of top quark couplings that can not be made using unpolarized pair-produced top quarks.

5 Electroweak Physics

The high value of the production cross-section for W and Z at the Tevatron, allows accumulation of large data samples and therefore allows precise tests of the Standard model (see Table 3 and Fig. 4). The Electroweak measurements are some of the most precise performed at DØ.

Table 3: Number of W and Z events observed in Run 1A

Channel	W	Z	$\int \mathcal{L} dt (pb^{-1})$
e	10338 events	775 events	12.8
μ	1665 events	77 events	11.4

5.1 W Mass Measurement

The measurement of the W boson mass M_W is one of the critical measurements for hadron collider experiments. This precision measurement, combined with the Z boson mass, width and decay asymmetries from the e^+e^- collider experiments, overconstrains the Standard Model. In addition, the value of the W mass, combined with the top quark mass will begin to place constraints on the Higgs mass.

We have measured the M_W using electron events; the signal is a high p_T electron with large \cancel{E}_T arising from the non-interacting neutrino. Since the neutrino's momentum along the incoming beam direction is not measured, the transverse mass

$$M_T^W = \sqrt{2p_T^l p_T^\nu (1 - \cos\phi_{l,\nu})} \quad (3)$$

is the experimentally reconstructed quantity. Here $\phi_{l,\nu}$ is the azimuthal angle between the lepton and the neutrino direction. M_W is measured by fitting the data M_T^W spectrum with a set of M_T^W template distributions generated from Monte Carlo simulation with different input M_W . The best fit to the M_T^W spectrum is shown in Fig. 5.

Crucial to this measurement is the understanding of the hadronic and electromagnetic energy scales. These effects are studied using the $Z \rightarrow e^+e^-$ events. The kinematics of the Z and W

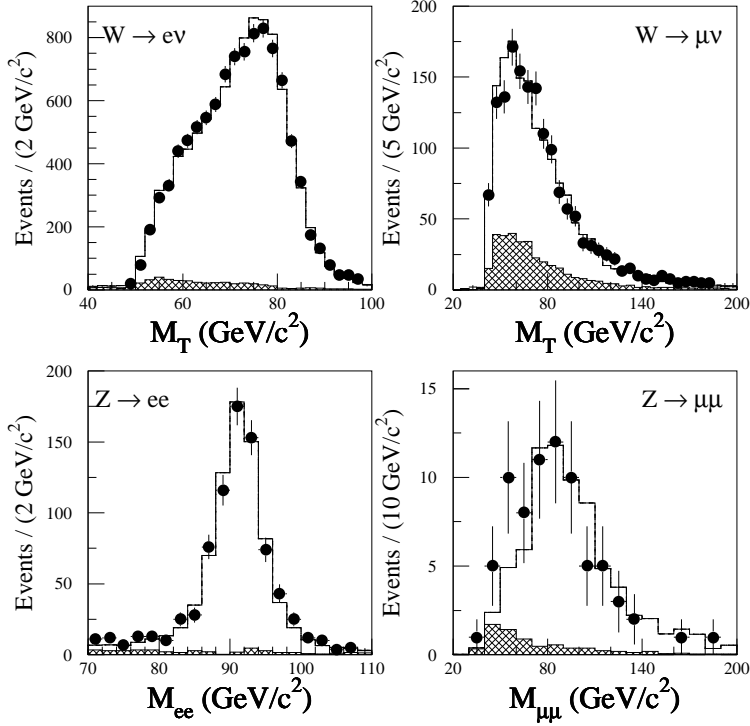


Figure 4: Transverse mass and invariant mass distribution. The points are for data. The shaded areas represent the estimated background and the solid lines correspond to the sums of the expected signals and the estimated backgrounds.

decays are similar, but since both decay leptons are observed in Z events, the requirement that the transverse momentum of the dilepton pair balance the recoiling hadronic system fixes the hadronic energy scale.

Our Z mass measurement combined with the observed positions of the π^0 and $J/\Psi \rightarrow e^+e^-$ mass peaks determines the electromagnetic scale factor and limits the non-linearity.

In 1994 $D\bar{O}$ presented a preliminary result from the Run 1A data representing a luminosity of $\approx 14 \text{ pb}^{-1}$ from a sample of 4817 events $W \rightarrow e\nu$, with the electron detected in the central calorimeter:

$$M_W = 79.86 \pm 0.16(\text{stat}) \pm 0.17(\text{syst}) \pm 0.26(\text{scale}). \quad (4)$$

The statistical error for the complete run 1A data sample is estimated to $\approx 150 \text{ GeV}/c^2$. Many studies are being performed to understand systematic errors. The energy scale error has been reduced to $\approx 170 \text{ GeV}/c^2$. A final result for M_W is expected soon.

The world average (UA1,UA2,CDF, $D\bar{O}$) for the error on the M_W will be $\approx 180 \text{ GeV}/c^2$ restricting the Tevatron results to run 1A data. This error is expected to decrease by a factor ≈ 2 when the full statistic of run 1A and run 1B is analysed. Another factor 2 reduction is expected when the Main Injector comes into operation (Fig 6).

D0 Preliminary: $W \rightarrow e \nu$ Decays(CC only)

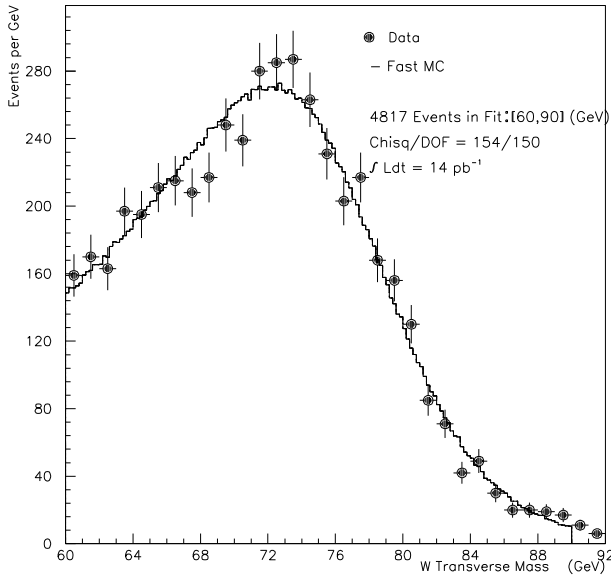


Figure 5: Fit to the W transverse mass electron data.

Scaling of W -mass error

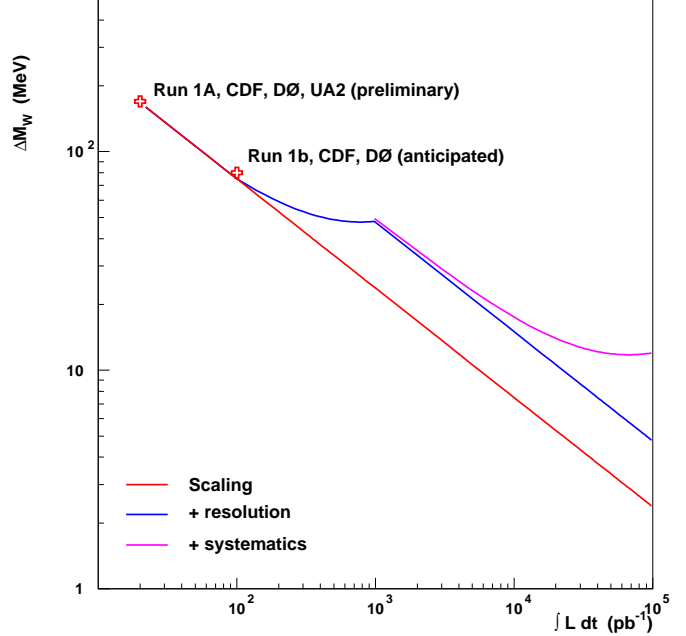


Figure 6: Uncertainty on M_W as a function of integrated luminosity.

5.2 W and Z Production Cross-sections

The production cross-sections of the W and Z bosons are measured by detecting the bosons through their decays into electrons or muons[12].

$$\begin{aligned}\sigma Br(W) &\equiv \sigma(p\bar{p} \rightarrow W) \cdot Br(W \rightarrow l\nu), \\ \sigma Br(Z) &\equiv \sigma(p\bar{p} \rightarrow Z) \cdot Br(Z \rightarrow l^+l^-).\end{aligned}$$

The ratio of these quantities, combined with LEP measurements of the Z widths and Standard Model calculations of the W partial width to leptons, can be used to derive the total width of the W boson, Γ_W .

$$\begin{aligned}R &= \frac{\sigma Br(W)}{\sigma Br(Z)} \\ &= \frac{\sigma(p\bar{p} \rightarrow W)}{\sigma(p\bar{p} \rightarrow Z)} \cdot \frac{\Gamma_Z}{\Gamma(Z \rightarrow l^+l^-)} \cdot \frac{\Gamma(W \rightarrow l\nu)}{\Gamma_W}\end{aligned}$$

This method gives the most precise measurement of Γ_W . The results from the cross-sections, based on the complete Run 1A data samples, are summarized below. These numbers will improve soon because of better understanding of the luminosity.

The $D\bar{O}$ measurement of the W width derived from the combined value for R is

$$\Gamma(W) = 2.044 \pm 0.093(stat + syst) GeV. \quad (5)$$

The world average prior to this measurement was $2.08 \pm 0.07 GeV$. The agreement of the measured width with the Standard Model prediction, $\Gamma(W) = 2.077 \pm 0.014$, can be used to set limits on

Channel	$\sigma Br(W)$ (nb)	$\sigma Br(Z)$ (nb)	R
D \emptyset e	$2.38 \pm 0.07 \pm 0.29$	$0.220 \pm 0.011 \pm 0.026$	$10.82 \pm 0.41 \pm 0.29$
D \emptyset μ	$2.12 \pm 0.23 \pm 0.25$	$0.180 \pm 0.031 \pm 0.022$	$11.8_{-1.4}^{+1.8} \pm 1.1$
combined			10.90 ± 0.49

non-standard W decay modes. For example, if there were a new quark coupling to the b quark with standard couplings, it would be excluded for masses below 61 GeV at the 95% confidence level.

5.3 Diboson Production and Anomalous Coupling Limits

The study of the $WW\gamma$ anomalous coupling provides an opportunity to test the self interactions of the gauge bosons, thus uniquely testing the Standard Model (SM) of the electroweak interactions. In the SM, the magnetic dipole moment and electric quadrupole moment of the W , are related to the CP conserving coupling constants κ and λ between the charged gauge vector bosons and photons by:

$$\mu_W = \frac{e}{2M_W}(1 + \kappa + \lambda)$$

$$Q_W = -\frac{e}{M_W^2}(\kappa - \lambda)$$

The CP violating couplings $\tilde{\kappa}$ and $\tilde{\lambda}$ are predicted to be 0 within the Standard Model[46]. Anomalous coupling parameters differ from zero only in extensions to the Standard Model. If they are non-zero, the cross sections will be larger and the kinematic distributions enhanced in the high p_T region.

The trilinear coupling of Electroweak gauge bosons is investigated through studies of production and characteristics of events having pair-produced bosons ($W\gamma$, $Z\gamma$, WW , and WZ)[11].

The event selection required a high P_t isolated lepton a high E_t isolated photon and large missing E_t (\cancel{E}_t)

For $\int \mathcal{L} dt \approx 13.4 pb^{-1}$ Run 1A provided a sample of[10]:

- 23 $W\gamma$ candidates (11 $W(e\nu)\gamma$, 12 $W(\mu\nu)\gamma$) with an estimated background of ≈ 6.4 events (Figure 7).
- 6 $Z\gamma$ candidates (4 $Z(ee)\gamma$, 2 $Z(\mu\mu)\gamma$) with an estimated background of ≈ 0.48 events.

The limit at 95% CL on anomalous vector boson couplings are the following:

$W\gamma(\Lambda = 1.5 \text{ TeV})$

$$-1.6 < \Delta\kappa < 1.8 \text{ for } \lambda = 0$$

$$-0.6 < \lambda < 0.6 \text{ for } \Delta\kappa = 0$$

$Z\gamma(\Lambda = 0.5 \text{ TeV})$

$$-1.8 < h_{30}^Z < 1.8 \text{ for } h_{40}^Z = 0$$

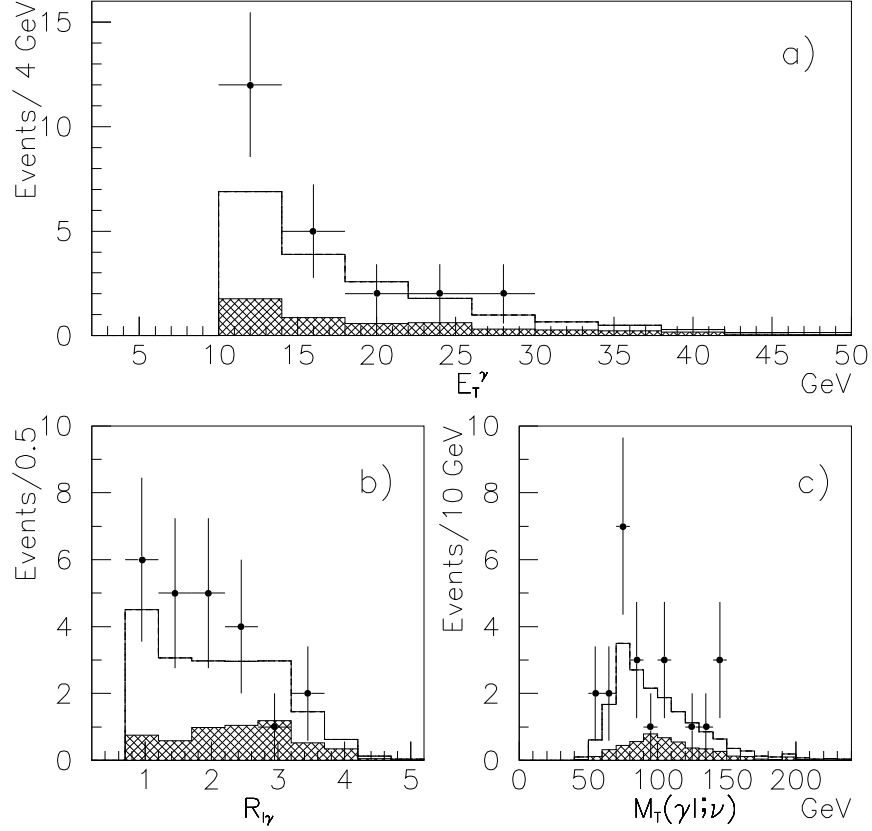


Figure 7: Distribution of (a) E_T^γ , (b) $R_{l\gamma}$ and (c) $M_T(\gamma l \nu)$ for the $W(e\nu)\gamma$ and $W(\mu\nu)\gamma$ combined sample. The points are the Run 1A data. The shaded areas represent the estimated background, and the solid histograms are the expected signal from the Standard Model plus the estimated background. $R_{l\gamma}$ is the separation in η, ϕ space between the lepton and the photon.

$$-1.5 < h_{40}^Z < 0.5 \text{ for } h_{30}^Z = 0$$

The distribution of the photon transverse energy, the angular separation of the photon from the decay lepton and the three-body transverse mass of photon, lepton and neutrino from leptonic decays of $W\gamma$ events are shown in Fig. 7a) - c). The pure $U(1)$ electromagnetic coupling of the W boson to the photon is excluded at 80% C.L.

A new topic for the Tevatron experiments is the study of W boson pair production. The accumulated data prior to collider Run 1A did not provide sensitivity to the relatively low cross-section of this process. Using the Run 1A data, DØ found one WW candidate with an expected background of about 1/2 of an event[9]. This topic is especially novel because the $t\bar{t}$ background must be removed. This analysis produced the following limit:

$$\begin{aligned}
WW(\Lambda = 1.5 \text{ TeV}) \\
-0.89 < \Delta\kappa < 1.07 \text{ for } \lambda = 0 \\
-0.66 < \lambda < 0.67 \text{ for } \Delta\kappa = 0
\end{aligned}$$

Our measurement of the Diboson production is in agreement with the Standard Model predictions, within the experimental sensitivity. The larger luminosity available in Run 1B will allow detailed studies of the kinematic distributions in $W\gamma$ and $Z\gamma$ events, may permit the first observation of the expected amplitude-zero in the $W - \gamma$ angular distribution. We expect to produce a clear sample of WW events, allowing improved trilinear coupling measurements.

6 Strong Interaction Physics

Strong interactions, those responsible for the bound states of nuclei and interactions between quarks, are perhaps the most difficult interactions to characterize using existing theory predictions. The difficulty arises from the inherent complexity of the calculations involved. Thus, experimental results are necessary to assess the reliability of various approximation schemes used to make predictions of strong interaction effects. The DØ research in this area covers a wide range of topics, the following of which are discussed here:

- Jet production
- Jet shape studies
- Color coherence
- Color singlet exchange
- Dijet decorrelation
- Inclusive photon production
- W+Jet production

6.1 Jet Production

Inclusive central jet production has been measured at several center of mass energies and shown to be in excellent agreement with next-to-leading order (NLO) Quantum Chromodynamics (QCD). The hermetic coverage of the DØ detector extends this measurement to forward angles and as such is a rigorous test of QCD near the kinematic limits.

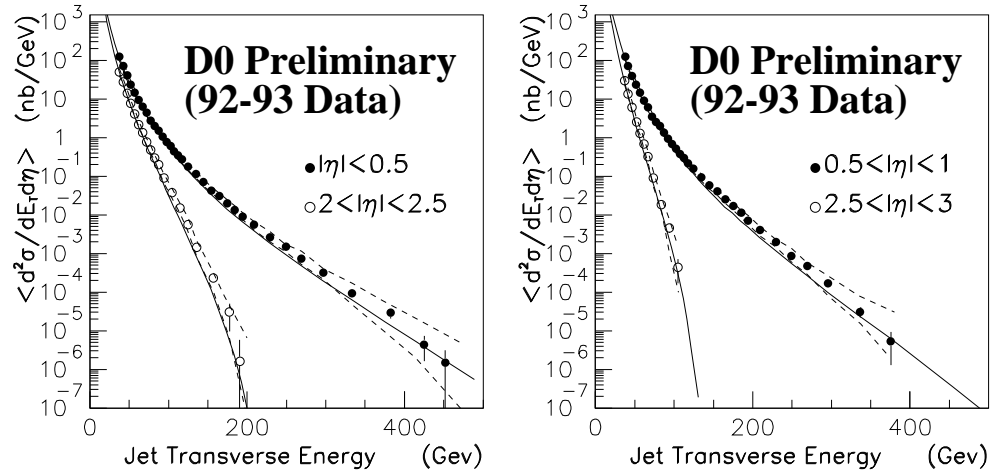


Figure 8: Inclusive jet cross section for several η bins.

As shown in Figure 8, the data agree within systematic errors (dashed lines) at all pseudorapidities (η) with the NLO calculations (solid lines). This agreement spans seven orders of magnitude of transverse energy for central jet production and five orders of magnitude for very forward jet production. One goal of our analysis is the measurement of Parton Distribution Functions (PDFs) using correlations between the leading (largest transverse energy) two jets.

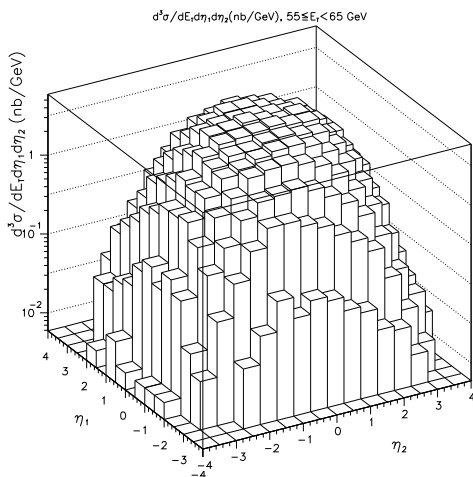


Figure 9: Triple differential cross section as a function of η_1 and η_2 for one E_T bin.

If NLO calculations give an adequate description of jet production, the dijet cross sections can

provide information on the parton distribution functions. Measurement of high rapidity final state jets is necessary to reach extreme values of parton x . Figure 9 shows a Lego plot of the triple differential cross section as a function of η_1 and η_2 of the two largest transverse energy (E_T) jets with the leading jet E_T integrated over 45 to 55 GeV. [18] The sharp fall-off at large rapidities is mostly due to the lack of partons at high x .

6.2 Jet Shape

Calculations at the parton level, which ignore fragmentation, describe many experimental processes, including inclusive jet and dijet production. We have tested whether NLO partonic QCD predictions can accurately describe the shape of a jet by measuring the transverse energy flow within jets [15].

The jet shape is characterized by the variable $\rho(r)$, defined as the fraction of transverse energy within the subcone of radius $r = \sqrt{\delta\eta^2 + \delta\phi^2}$. Jets are divided into ten subcones around the jet axis with radii varying from 0.1 to 1.0.

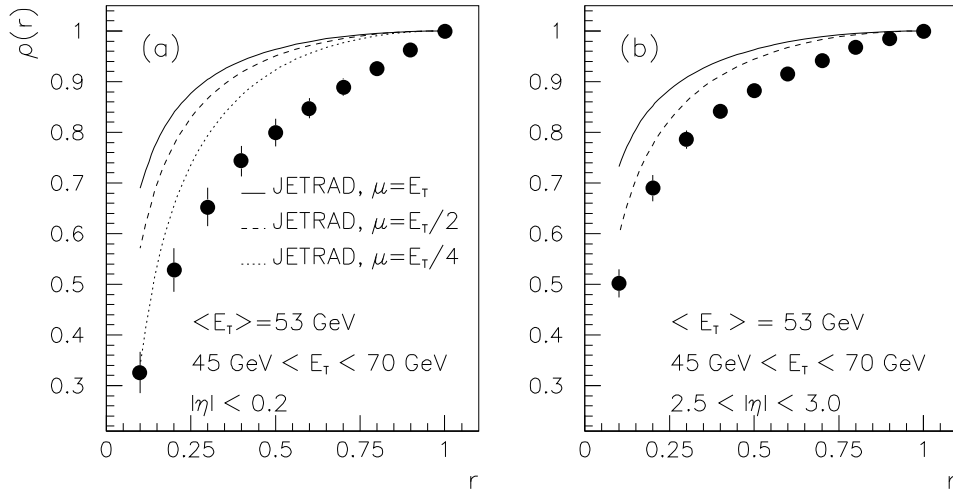


Figure 10: Jet shape for data (dots) and NLO prediction (curves) in central(a) and forward(b) η bins.

Figure 10 compares the experimentally measured jet shape to NLO predictions (JETRAD) for different renormalization scales, μ , in two different η regions. We see that NLO jet shape predictions are unable to accurately describe the experimentally measured jet shape independent of scale choice.

Future analyses in this area will include comparisons to jet shapes measured at e^+e^- experiments. Preliminary results show jets at e^+e^- experiments to be narrower than jets produced at $p\bar{p}$ colliders. Monte Carlo studies have shown quark jets to be much narrower than gluon jets. Since many more gluon jets are produced at $p\bar{p}$ colliders, this may explain the difference in shape between jets produced in $p\bar{p}$ collisions and in e^+e^- collisions. Investigations of quark and gluon jet differences in the experimental data are underway, and it may be possible to discriminate between quark and gluon jets with reasonable efficiency.

6.3 Color Coherence

Initial and final state color coherence effects in $p\bar{p}$ collisions are studied by measuring spatial correlations between soft and hard jets in multijet events. This analysis provides insight into strong-interaction interference between the initial and final state particles. This analysis requires that events have three or more jets with $E_T > 15$ GeV and the leading jet $E_T > 120$ GeV. Jets are ordered in E_T , and the two leading jets required to be in opposite ϕ hemispheres.

The angular distribution of the softer third jet around the second highest E_T jet in (η, ϕ) space is studied using the angular variable β , measured in the plane defined by the second jet and the beam. The beam directions correspond to $\beta = 0, \pi$, and $\beta = \frac{\pi}{2}, \frac{3\pi}{2}$ correspond to the directions perpendicular to the beam. The expectation from initial-final state color interference is that the rate of soft jet emission in the regions $\beta = 0, \pi$ will be enhanced with respect to that in the region $\beta = \frac{\pi}{2}, \frac{3\pi}{2}$.

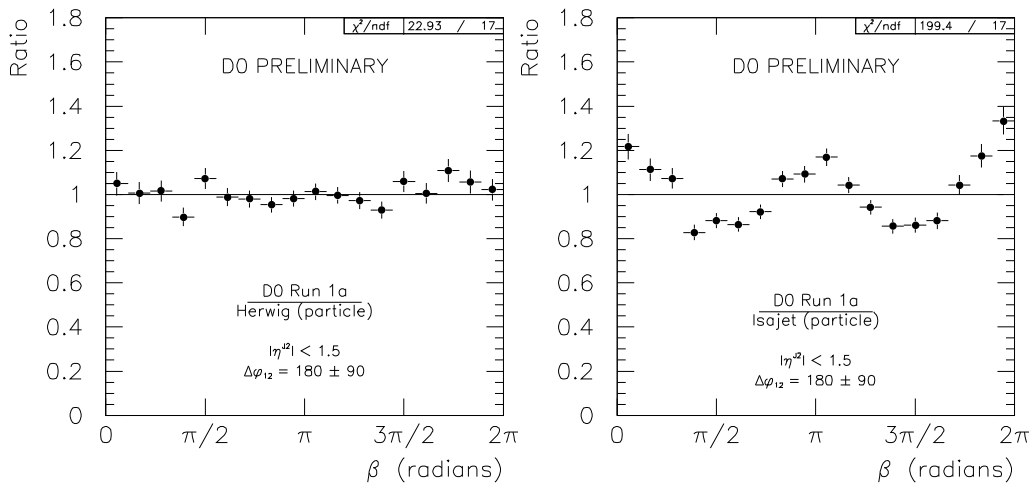


Figure 11: Comparison of the β variable showing location of third jet between data and the HERWIG and ISAJET Monte Carlos.

The data angular distributions are compared with two shower Monte Carlo event generators (ISAJET and HERWIG) that differ in their implementation of color coherence. Figure 11 shows the ratio of the β distributions between data and the two simulations when the second jet is constrained to $|\eta| < 1.5$. ISAJET which uses an independent shower development model (no color coherence effects are included) clearly disagrees with the data, whereas HERWIG, which incorporates color coherence effects by means of an angular ordering approximation of soft gluon radiation, is in qualitative agreement with the data. Complementary analyses are under way to study the color coherence effects of soft gluon radiation by measuring the energy flow patterns in W +jet, γ +jet and jet+jet event samples.

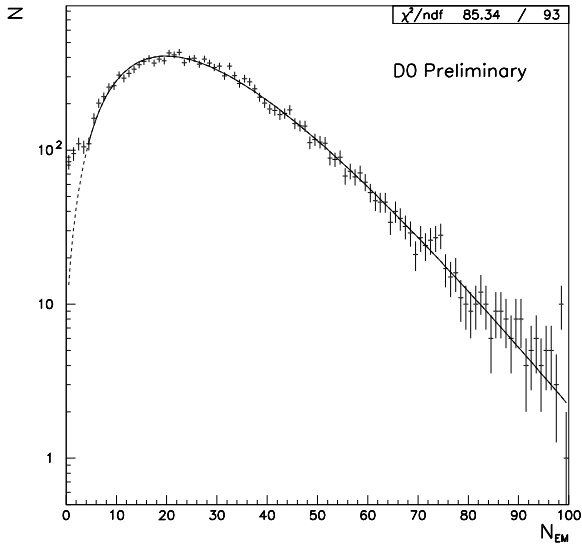


Figure 12: Tower multiplicity between jets with large pseudorapidity separation compared to negative binomial fit.

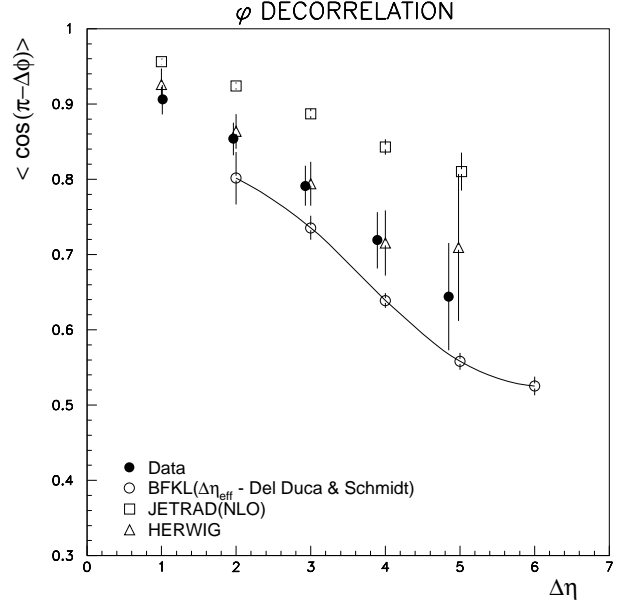


Figure 13: $\langle \cos(\pi - \Delta\phi) \rangle$ versus $\Delta\eta$ for data compared to JETRAD, HERWIG, and BFKL predictions.

6.4 Color Singlet Exchange

In this analysis we search for strongly interacting color singlet exchange by tagging events with a low multiplicity of particles between jets[5],[19]. Few particles are expected between the leading jets in color singlet events, whereas the presence of a color string connecting the scattered partons in color octet events (gluon exchange) gives rise to a smooth distribution of particles between the leading jets. The color octet multiplicity distribution can be parameterized by a Negative Binomial (NB) distribution. Control samples taken from data and Monte Carlo support this parameterization. An excess of events over the NB fit at low multiplicity signals the presence of color singlet exchange.

Figure 12 shows the multiplicity of electromagnetic calorimeter towers with $E_T > 200$ MeV (the $D\bar{O}$ method of tagging particles) between the leading jets of an inclusive dijet sample in which the leading jets are separated by at least 4.4 units in rapidity. The large rapidity separation between the leading jets reduces the probability that a color octet event will produce a small number of particles in the region between the jets. There is a clear excess of the data over the NB fit at low multiplicity. The fractional excess in bins of multiplicity 0 to 3 is $1.5 \pm 0.2\%$ which is two orders of magnitude above expectations from electroweak exchange, and of the same order as rough theoretical estimates of Pomeron exchange by Bjorken and others. This result suggests the presence of a strongly interacting color singlet exchange. Further analyses studying the transverse momentum dependence of color singlet production as well as different rapidity gaps configurations are underway.

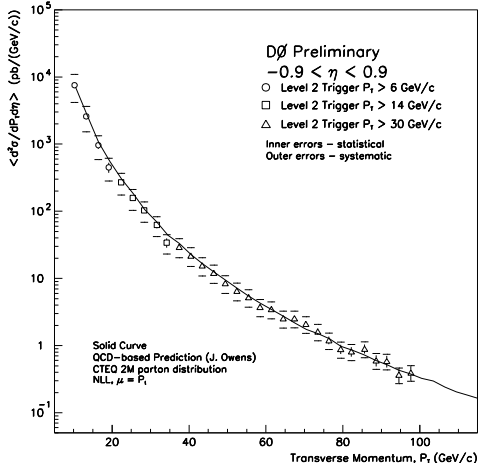


Figure 14: Inclusive photon cross section compared to the QCD prediction

6.5 Dijet Decorrelation

We study the decorrelation in azimuthal angle between dijets as a function of the pseudorapidity separation between the jets. The variable of interest, $\langle \cos(\pi - \Delta\phi) \rangle$, is unity for completely correlated (back-to-back) jets and zero for uncorrelated jets. Decorrelation is expected to arise due to soft gluon emissions in the rapidity interval between the jets. The $D\phi$ data is compared with a NLO Monte Carlo (JETRAD), a shower Monte Carlo (HERWIG), and the theoretical prediction of Del Duca and Schmidt which is based on BFKL resummation techniques.

The comparison is shown in Figure 13. The data show a significant decorrelation as the rapidity separation increases. HERWIG shows a decorrelation trend similar to the data, while the NLO prediction underestimates the decorrelation and the BFKL prediction overestimates it.

Detector effects and the cone size dependence studies are still in progress. Also, an analysis with lower E_T jets allowing a larger rapidity interval is underway.

6.6 Inclusive Photon Production

Direct photons provide an interesting probe of QCD because, unlike jets, they are not subject to final state interactions, they can be relatively unambiguously identified, and their energy is measured accurately. Unfortunately, photons also suffer from a large background due to electromagnetically-fragmenting jets.

Photon candidates with transverse momentum greater than 9 GeV/c and within $|\eta| < 0.9$ were selected by requiring isolated showers contained in the EM calorimeter, with a shape consistent with the one measured for an electron in a test beam, and no associated track in the central tracking chambers. The background contribution has been estimated using the longitudinal and transverse shower shape, and by measurement of photon conversions probability in the central track detector.

A preliminary measurement of the cross section for the inclusive production of central, isolated direct photons is shown in Figure 14: the photon cross section is in good agreement with the next-to-leading order QCD calculation of Owens *et al.*

7 Results from Searches for New Phenomena

A number of searches for phenomena beyond the Standard Model have been pursued using the data from Run 1A. These searches are now being extended to include the Run 1B data, and additional topics accessible with the increased luminosity of Run 1B are also under study.

The range of searches has led to:

- A mass limit on first generation scalar leptoquark. This was the first published Run 1A $D\bar{O}$ physics result.
- A mass limit on the second generation leptoquark.
- Limits on the masses of squarks and gluinos, within the context of the Minimal Supersymmetric Standard Model (MSSM).
- Cross section times branching fraction limits on gaugino production in the MSSM context.
- Limits on the masses of heavy W and Z bosons.
- Limits on the masses of a heavy right-handed W and its associated (heavy) neutrino.

Also completed is a search for indications of compositeness in events with high scalar transverse energy. This will be translated to limits on the compositeness scale soon.

These searches will be extended by additional data from Run 1B. Additional searches for b' quarks, heavy neutral leptons, charged and neutral Higgs particles, massive stable particles, and other exotica are being pursued.

So far, however, only limits are reported— no new phenomena have been seen.

7.1 Leptoquarks

Leptoquarks (LQ) are exotic particles with both color and lepton quantum numbers. They mediate an interaction between leptons and quarks. The coupling strength for LQ masses reachable at the Tevatron is expected to be about 0.1α . The decay length for the LQ are expected to be short so they should be easily observed in the detector. The first generation leptoquarks (LQ1) are expected by definition to couple only to electrons, electron neutrinos, up and down quarks. The second generation leptoquarks (LQ2) couple only to muons, muon neutrinos, charm and strange quarks. The HERA mass limit for scalar LQ1 is 240 GeV for a leptoquark coupling equal to the electroweak coupling α , and drops to LEP limit of 45 GeV at a coupling of 0.05α .

Leptoquark production is dominated by pair production through gluon-gluon fusion and $q\bar{q}$ annihilation. We assume that the leptoquark decays to lepton plus quark with a branching fraction of β , and to neutrino plus quark with a branching fraction of $(1 - \beta)$.

The signatures will be: 2 jets + l^+ + l^- , 2 jets + l^\pm + \cancel{E}_T , 2 jets + \cancel{E}_T .

We have conducted searches in the first two channels for first and second generation leptoquarks. The results for the first generation search have been published [2].

The excluded region for the first generation LQ is shown in Figure 15 and the limits are: $M_{LQ1} > 130$ GeV for $\beta = 1.0$, and $M_{LQ1} > 116$ GeV for $\beta = 0.5$.

The second generation search is based on $12.7 \pm 0.67 pb^{-1}$ of data from the 1992-1993 running period [42, 43]. The trigger, based on muons plus jets, requires at least one μ with $p_T > 8$ GeV and

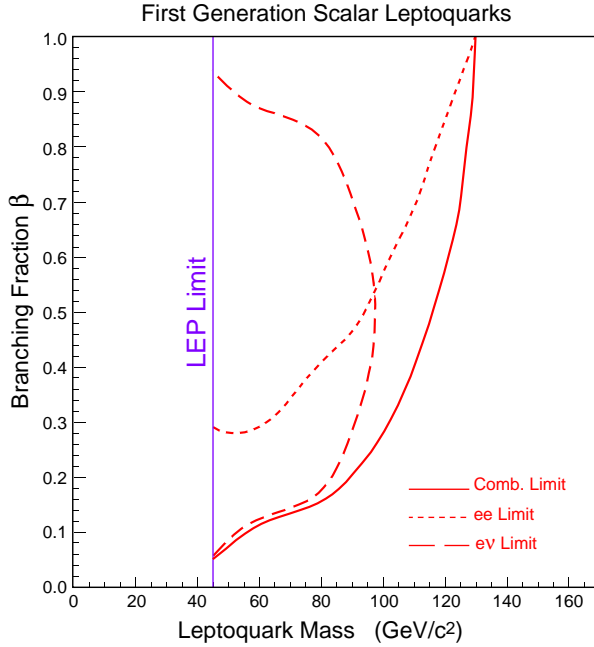


Figure 15: The 95% CL First generation Leptoquark Mass excluded region vs. branching fraction.

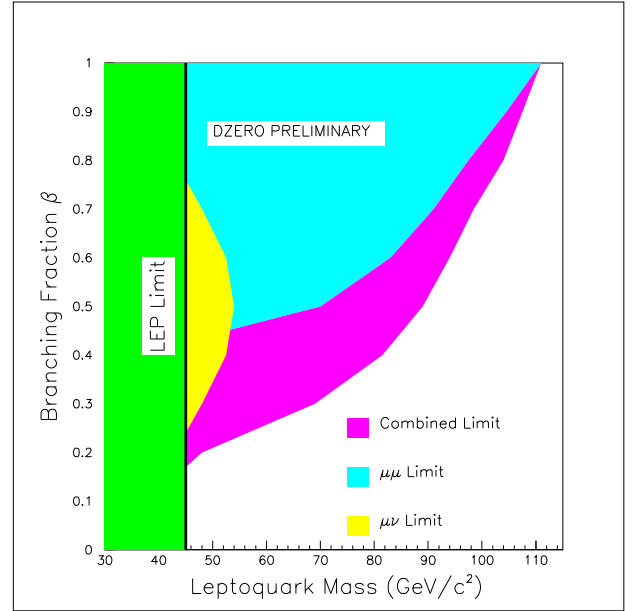


Figure 16: The 95% CL Second generation Leptoquark Mass excluded region vs. branching fraction.

one jet with $E_t > 15$ GeV. Cuts are made to reduce backgrounds from W and Z bosons plus jets, $b\bar{b}$ production and cosmic rays. No candidates remain after all cuts are imposed, with an expected background of 1.8 ± 0.7 events. The largest background is from $W \rightarrow e\nu$ which is reduced with the transverse mass cut. No events are observed with an expected background of 2.4 ± 1.0 events.

We interpret a null search as a limit on $\sigma\beta^2$. Using the cross section calculations obtained using ISAJET with Morfin and Tung leading order pdf for pair produced scalar leptoquarks, we determine a β dependent limit on the LQ mass. The excluded region is shown in Figure 16. The 95%CL mass limits are $M_{LQ2} > 111$ GeV for $\beta = 1.0$, and $M_{LQ2} > 89$ GeV for $\beta = 0.5$. Including the run 1b data we expect to be able to increase the LQ1 and LQ2 mass limits significantly.

7.2 Search for Supersymmetric particles

Among the leading theoretical models which require extensions to the Standard Model are the various super symmetry (SUSY) theories. These theories address the fundamental asymmetry between the fermionic quarks and leptons and the bosonic force carriers by hypothesizing the existence of bosonic quarks and leptons and fermionic force carriers.

Many new particle states are predicted as part of the Minimal Supersymmetric Standard Model. These include Supersymmetric partners of quarks (squarks), leptons (sleptons), and of the gauge and Higgs bosons (gauginos). There are two Higgs doublets, the ratio of their Vacuum Expectation Values is called $\tan(\beta)$. There is a quantity called R-parity which is +1 for normal standard model particles and -1 for SUSY states. If R-parity is conserved then SUSY particles can only be created in pairs and the lightest SUSY particle, the \tilde{Z}_1 (sometimes referred to as the $\tilde{\chi}_1^0$), must be stable

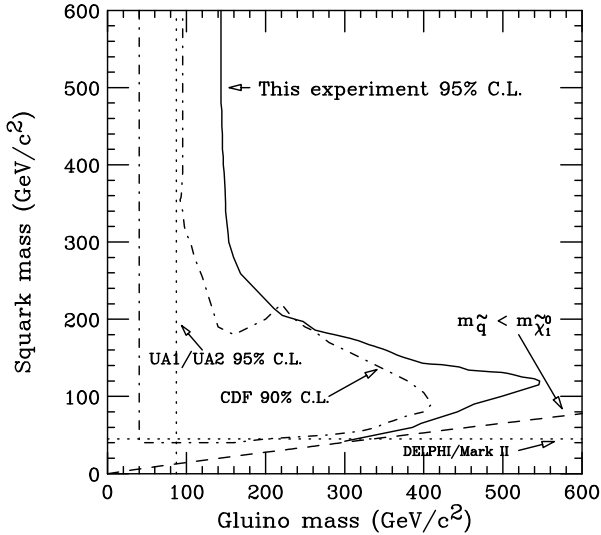


Figure 17: Current squark and gluino mass limits. Left of the dot-dashed line is the gluino mass region excluded by UA1 and UA2. Below the dotted line is the squark mass region excluded by the LEP experiments. Inside the dashed line is the CDF 90% confidence level excluded region. Below the solid line is the DØ 95% confidence level excluded region.

and unobservable. The next lowest mass state gauginos are predicted to be a chargino \tilde{W}_1 (or $\tilde{\chi}_1^+$) and a neutralino \tilde{Z}_2 (or $\tilde{\chi}_2^0$).

The models can be stretched over a very wide phenomenological space and have very few experimental constraints. However, the most constrained of these models are likely to be accessible at the Tevatron.

7.2.1 The Squark/Gluino Search

Evidence for squarks (the super symmetric partners of quarks) and gluinos (the super symmetric partners of gluons) is searched via their hadronic cascade decays.

The signal would have multiple jets and significant \cancel{E}_T , arising from the escape of the weakly interacting, stable, lightest super symmetric particle (LSP) at the end of the decay chains.

After strict requirements on the jets and $\cancel{E}_T > 75$ GeV, the background from multijet events with fluctuations in the measured jet energies is negligible, and the number of events seen (14 events with 3 jets and 5 events with 4 jets), and their distribution in \cancel{E}_T , is well predicted by the estimated background from vector bosons + jets(14.2 ± 4.4 and 5.2 ± 2.2 respectively).

For very heavy squarks the preliminary 95 % CL lower mass on the gluino mass is $m_{\tilde{g}} > 173$ GeV/ c^2 . If squarks and gluinos have equal mass, the 95 % CL limit is $m_{\tilde{g}} > 229$ GeV/ c^2 [3].

7.2.2 The Wino/Zino Search via Trilepton Final States

One possible favorable gaugino production method at the Tevatron is through an s channel off-shell W which produces a chargino-neutralino pair [38] shown in Figure 18. These in turn decay to produce the following states: 4 jets + \cancel{E}_T , 1 lepton + 2 jets + \cancel{E}_T , 2 Leptons + 2 jets + \cancel{E}_T , 3 leptons + \cancel{E}_T , where \cancel{E}_T is the transverse energy imbalance of the event. Of particular interest is the tri-lepton final state which is expected to have very low backgrounds. The p_T distributions of the three leptons have been studied using Monte Carlo simulation [39], and show that the lowest p_T lepton has a very soft spectrum and requires a low cut on p_T .

The search has been conducted with 12.2 pb^{-1} from the run 1A data [40]. The triggers used to collect this sample were based on one high p_T lepton or two low p_T leptons. Offline filtering

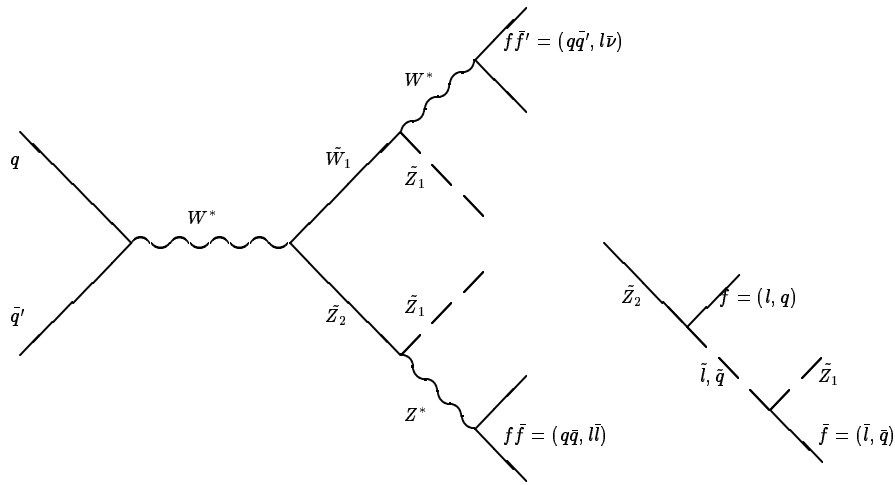


Figure 18: Feynman diagrams showing the \tilde{W}_1 \tilde{Z}_2 production and decay.

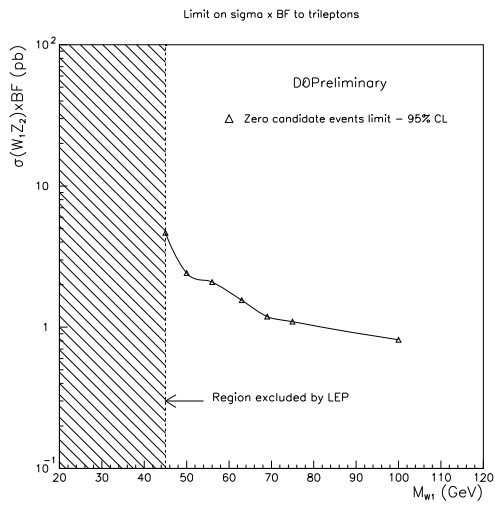


Figure 19: The 95% CL on cross section times branching fraction $\tilde{W}_1 + \tilde{Z}_2$ plus \cancel{E}_T final state, as a function of $M_{\tilde{W}_1}$.

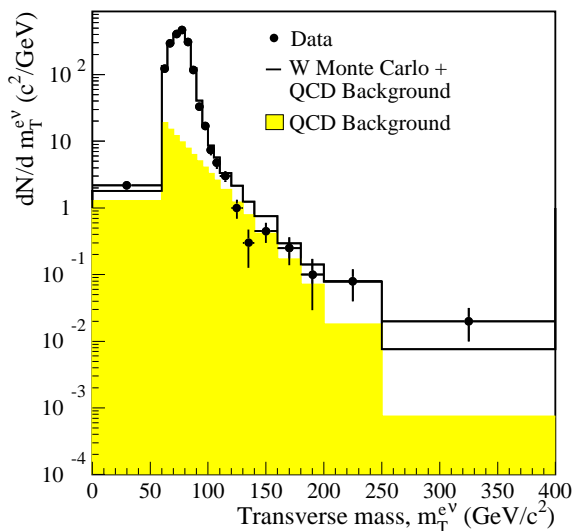


Figure 20: Electron-neutrino transverse mass distribution for data compared to W Monte Carlo plus QCD background.

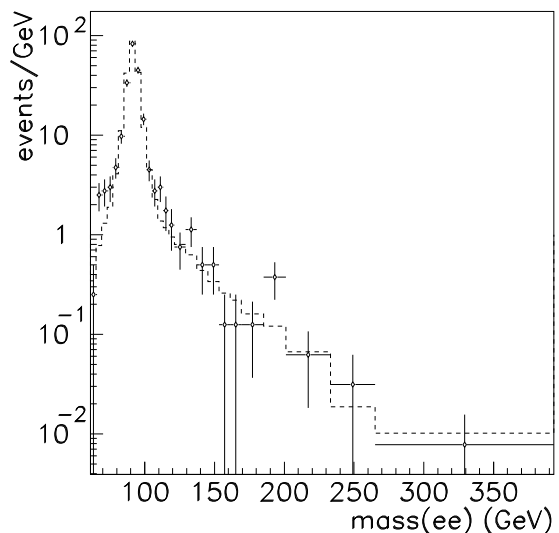


Figure 21: Observed dielectron events (discrete points) are compared to the combined Z -Drell-Yan and QCD background.

further tightens the cuts imposed by the triggers. There are four channels which are analyzed separately: $eee, ee\mu, e\mu\mu$ and $\mu\mu\mu$. No candidates remain in any channel after all cuts are made. The backgrounds include Drell-Yan and $Z \rightarrow \bar{l}l + \gamma$, Drell-Yan and $Z \rightarrow \bar{l}l + jet$, $W + 2$ jets, $WZ \rightarrow 3$ leptons, $b\bar{b}$, and QCD 3 jet events.

The cross section limits for 95% confidence level (CL) are shown in Figure 19. With further improvements in cut efficiencies these limits should be lowered by 30% or more. With the additional data from the run 1b data set, more than 50 pb^{-1} will be added to the statistics. This will greatly improve our reach into the allowed parameter space of such models as, for example, the so-called "Constrained Minimal Supersymmetric Standard Model" [41].

7.3 The Search for heavy W and Z bosons

We have searched for a heavy charged gauge boson, W' , using the decay channels $W' \rightarrow e\nu$ and $W' \rightarrow \tau\nu \rightarrow e\nu\nu\bar{\nu}$ [16]. and for a heavy neutral gauge boson, using the decay channel $Z' \rightarrow ee$. The data used in the analysis correspond to an integrated luminosity of $13.9 \pm 0.8 \text{ pb}^{-1}$

Figure 20 shows the transverse mass $m_T^{e\nu}$ distribution and Figure 21 shows the dielectron invariant mass spectrum. Data is compared to the sum of Monte-Carlo predictions plus background. In both cases, the agreement is quite good.

In the region $m_T^{e\nu} > 150 \text{ GeV}/c^2$ there are 16 events in the data sample. Monte Carlo plus QCD predict 19.4 ± 5.7 events. In the region $m_T^{e\nu} > 250 \text{ GeV}/c^2$ there are three events in the data sample. Monte Carlo plus QCD predict 1.3 ± 0.4 events.

In the absence of Z' , for $m_{ee} > 200 \text{ GeV}/c^2$ we expect $4.2 \pm 0.3 Z\gamma^*$ plus QCD background events. Six events are observed in the data.

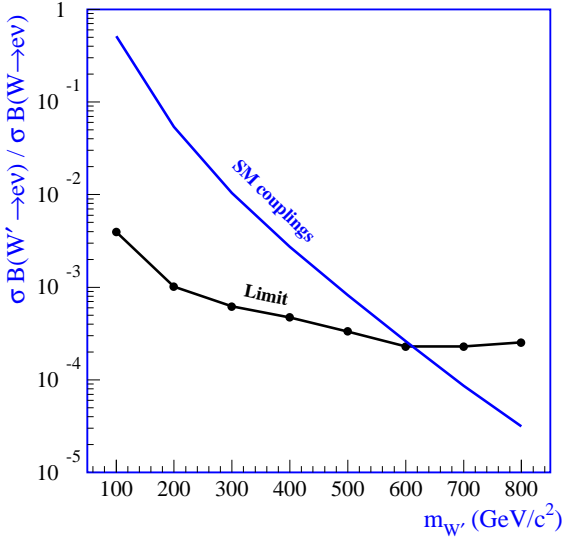


Figure 22: 95% C.L. upper limit as a function of $m_{W'}$ for $\sigma B(W' \rightarrow e\nu)/\sigma B(W \rightarrow e\nu)$.

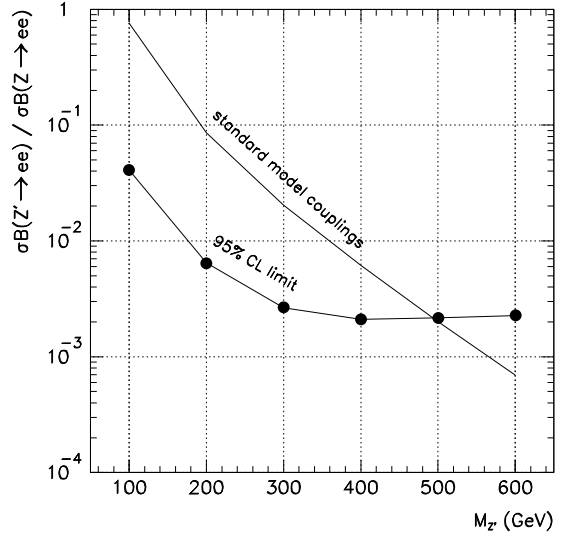


Figure 23: 95% CL upper limit as a function of $m_{Z'}$ for $\sigma B(Z' \rightarrow ee)/\sigma B(Z \rightarrow ee)$.

The 95% C.L. upper limit on $\sigma B(W' \rightarrow e\nu)/\sigma B(W \rightarrow e\nu)$ is plotted as a function of $m_{W'}$ in Figure 22 together with the theory curve, the value of this ratio assuming standard model couplings. A W' with the same couplings to quarks and leptons as the standard model W boson is excluded for $m_{W'} < 610 \text{ GeV}/c^2$.

The 95% C.L. upper limit on the cross section times branching ratio for $Z' \rightarrow ee$ is plotted as a function of m_{ee} in Fig. 23 together with the theory curve. We exclude the existence of a Z' of mass less than $490 \text{ GeV}/c^2$, assuming a reference model Z' with the same couplings to quarks and leptons as the standard model Z boson.

7.4 The Search for Compositeness via Events with Large Scalar E_T

Although the quarks and leptons are assumed in the Standard Model to be point-like objects, it is natural to test this assumption wherever possible. One method of testing this assumption is to search for evidence of compositeness in events with high energy flow in the plane perpendicular to the beam. This is a direct analogy with the Rutherford scattering experiments performed at the turn of century which lead to the discovery of the atomic nucleus.

A search for such events has been carried out. No evidence for departure from expected behavior has been seen, and this will soon be converted to a limit on the compositeness scale.

7.5 "bosonic" Higgs

In multi-Higgs-doublet models, it is possible for the Higgs which gives mass to fermions to be distinct from that which couples to bosons and which breaks EW symmetry. The latter can then have a very small coupling to fermions and decay predominantly to 2 photons for masses below

about 100 GeV, or to WW* for higher masses [44].

We have searched for such a "bosonic Higgs" in the associated production channel where the Higgs is produced together with a W or Z which decays to jets. We require two photons above 20 GeV, passing standard DØ photon cuts and with $|\eta| < 2.5$, and two jets above 15 GeV with an invariant mass between 65 and 105 GeV/c².

Data from Run 1A and part of run 1B were analysed for a total luminosity of 71.4 pb⁻¹. After all cuts 3 events were observed in the signal region ($m_{\gamma\gamma} > 60\text{GeV GeV}/c^2$) No events are observed with ($m_{\gamma\gamma} > 76\text{GeV}$)

The principal background is expected to be from QCD two jet plus two photon events, and QCD multi-jet events with some of the jets faking photons in the calorimeter. Using the theoretical cross section of Ref. [44] we set a preliminary lower limit on a bosonic Higgs mass of 73.5.5 GeV/c² at the 95% CL.

With the total statistics ($\int \mathcal{L}dt \approx 100\text{pb}^{-1}$) available, we anticipate to extend the reach of this search to about 90 GeV/c².

7.6 Summary

In conclusion, the searches completed thus far on Run 1A data have in many cases significantly extended limits on various new phenomena, but unfortunately have not given evidence yet for any effects or particles beyond the Standard Model. Much more remains to be done with these data and with the greatly increased luminosity from Run 1B, and such searches will be extended significantly.

8 *b*-Physics

The study of *b*-quark production at the Fermilab Tevatron provides an excellent testing ground for the details and procedures of perturbative *QCD* and will be of interest in coming *CP* violation studies in the *B* system. The relatively large *b*-quark mass implies that theoretical calculations may be more reliable than for other light-quark processes. Furthermore, because *b*-quark events can be experimentally separated from events without *b*-quarks, benchmark comparisons to theory in production cross sections and angular correlations can be performed.

Although the DØ detector has been optimized for high *p_T* physics, its extensive muon detection system combined with triggering capabilities on relatively low-energy muons makes it feasible to study *b*-physics as well. However, only muons with momentum above 3 GeV/c can penetrate to outer layers of the muon system. The lack of the central magnetic field in the present detector prohibits any studies of exclusive decay modes.

The hadroproduction of *b*-quarks has recently been a subject of intense studies, both theoretically and experimentally. The next to leading order (*NLO*) calculations have been available for some time. The lowest order *b \bar{b}* production processes (*s*-channel gluon diagrams or *t*-channel quark exchange) are rivaled at large *p_T* by $O(\alpha_s^3)$ diagrams including the *t*-channel gluon exchanges with subsequent gluon splitting and flavor excitation diagrams. Although earlier UA1 results were in reasonable agreement with *NLO QCD* calculations at $\sqrt{s} = 630$ GeV, more recent CDF results have tended to be roughly a factor of two higher than the theoretical central values.

The DØ *b*-physics studies have concentrated on:

- inclusive *b*-quark cross sections over a wide rapidity range.

- production mechanisms for the charmonium (J/Ψ and χ_c) and bottomonium (Υ) states,
- $b\bar{b}$ correlations,
- the heavy flavor content of jets.

8.1 Inclusive Cross-section Measurements

We have measured the b quark cross section using 3 independent data samples: single muons, non resonant dimuons and J/Ψ .

For the single muon analysis, based on $\int \mathcal{L} dt = 75.6 \pm 4.1 \text{ nb}^{-1}$, events were required to have at least one muon track with rapidity $|y^\mu| < 0.8$ and p_T^μ range 4–30 GeV/c. The muon cross section due to inclusive b quark decays was obtained by correcting for the total muon detection efficiency, the muon momentum resolution and for the measured fraction due to b decays[8].

For the dimuon sample, offline cuts were applied to select two muons in the kinematic range $|\eta^\mu| < 0.8$ and $p_T^\mu > 4.0 \text{ GeV}/c$, each muon associated with a jet with $E_T^{jet} > 12 \text{ GeV}$ within $\Delta R = 0.8$. The dimuon mass was restricted to be in the region $6 \text{ GeV}/c^2 < M_{\mu\mu} < 35 \text{ GeV}/c^2$ thus eliminating sequential decays of b quarks, J/Ψ decays, and Z decays. To reduce cosmic ray background, the opening angle between the two muons was required to be less than 165° . The inclusive J/ψ cross section determination, and the inferred integrated b quark cross section, was based on a restricted data sample of 1221 events, corresponding to a total integrated luminosity of 6.6 pb^{-1} . For this sample it was required that the events had two good muons and the pseudorapidity range for the dimuon was restricted to $|\eta| < 0.6$. The invariant mass distribution for opposite charge dimuons from the restricted data sample is shown in Figure 25. A strong J/Ψ signal is observed with a mass resolution well represented by a Gaussian function with a width of 380 MeV. The dominant contribution to the continuum is expected to come from processes involving heavy quarks: $b\bar{b}$ and $c\bar{c}$ events with both heavy quarks decaying semileptonically, sequential semileptonic decays $b \rightarrow c + \mu$, $c \rightarrow \mu$ as well as cases where one muon comes from a b or c decay and the other from a decay of a π or K meson. Other mechanisms that yield opposite sign dimuons are virtual photon decays, referred to as the Drell-Yan process, and the formation of light quark mesons, such as ρ , ϕ and η .

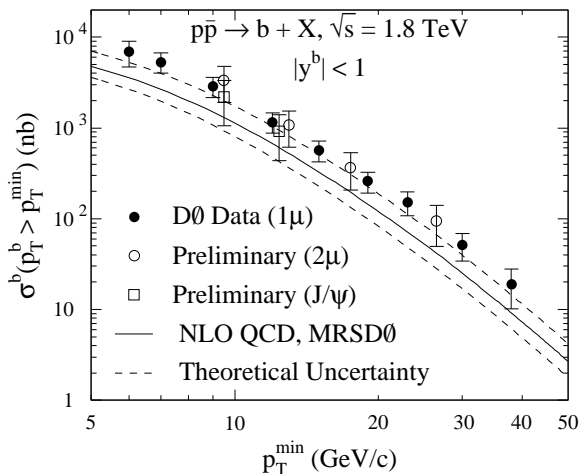


Figure 24: b -Quark Cross Section from inclusive muon, dimuon and J/Ψ .

In Figure 24 our measurements are compared to NLO QCD predictions using MRSD \emptyset parton distribution functions [45]. The QCD scale $\Lambda_{\overline{MS}}^{(5)} = 140$ MeV and the renormalization and factorization scale $\mu = \mu_0$ (with $\mu_0^2 = m_b^2 + (p_T^b)^2$, and $m_b = 4.75$ GeV/c²) were used for the solid curve, and customary variations of these parameters for the dashed curves: 187 MeV and $\mu_0/2$ (upper), and 100 MeV and $2\mu_0$ (lower).

Our results are consistent with the upper limit of the NLO QCD band, corresponding to the choice $\Lambda_{\overline{MS}}^{(5)} = 187$ MeV and the factorization - renormalization scale $\mu = \mu_0/2$.

Within errors, our b - *quark* cross section agrees with that of CDF for inclusive leptons. Thus, the data of both experiments favor smaller values of the renormalization and factorization scale μ .

8.2 Charmonium and Bottomonium Production

A $c\bar{c}$ state is the lightest bound system of quarks for which perturbative QCD is expected to apply. The J/Ψ is of particular significance because of its clean signature through the dilepton decay modes. In high energy $p\bar{p}$ collisions the dominant contributions to the J/Ψ production are expected to come from the lowest order Feynman diagrams with gluon-gluon fusion, either directly into charmonium and a recoiling gluon, or through a $b\bar{b}$ pair followed by a decay $b \rightarrow J/\Psi X$. It has been argued recently that, in addition to the gluon-gluon fusion, the process of gluon fragmentation, i.e. splitting of a virtual gluon into a charmonium state and other partons, is an important source of J/Ψ .

The fitted contributions to the dimuon spectrum from various processes is shown in figure 25. The total number of J/Ψ events is estimated to 407 ± 28 , of which 147 ± 33 are isolated. The fraction of J/Ψ events attributed to nonisolated production is 0.64 ± 0.11 .

In figure 26 the J/Ψ inclusive production cross section as a function of the transverse momentum is compared to the theoretical predictions [27].

Our measurement confirms the previous CDF cross section measurements[32]. The role of various production mechanisms has been investigated by using vertex information or requiring a third muon which is associated with the non- J/Ψ jet.

Measuring photons associated with J/Ψ 's can be used to estimate J/Ψ production from radiative χ_c decays. For example, the χ_c signal of 66 ± 15 events from the run 1A data is shown in Fig. 27. Photons from χ_c decays have energies of order 1 GeV and their reconstruction is a demanding technical test of the D \emptyset electromagnetic calorimeter performance. We estimate that $30 \pm 9\%$ of J/Ψ 's with $p_T > 8$ GeV/c and $|\eta| < 0.6$ are due to χ_c production. The Υ production cross section in the central region has been measured as well.

8.3 Summary

Many more analyses of the existing data are in progress. High statistics studies of dimuon and muon-opposite side jet correlations should provide new, more discriminating tests of the QCD calculations. Also, cross section measurements over the full pseudorapidity range ($|\eta| < 3.3$) will probe gluon structure functions at values of $x \approx 10^{-4}$.

The production of b -quarks is being actively investigated. With three to five times the data samples from the current collider run in hand, significant improvements in the quality and precision of QCD tests of heavy flavor production are expected.

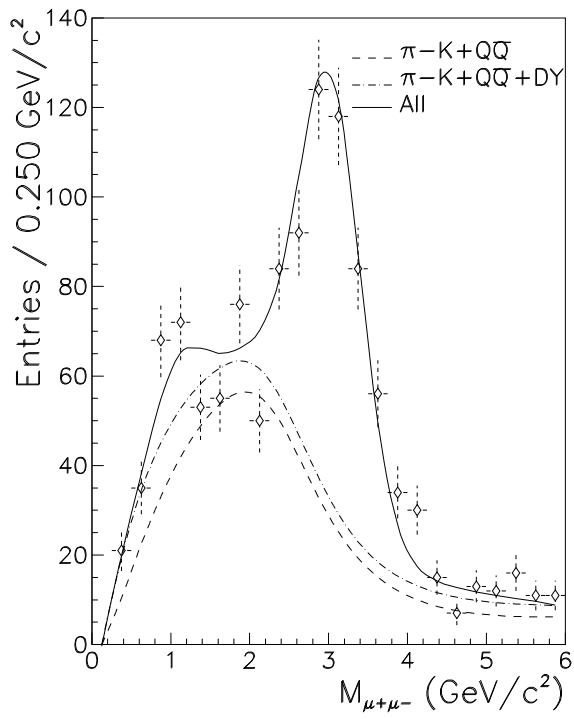


Figure 25: Dimuon Invariant Mass spectrum for opposite sign muons. The solid curve is the fitted sum of the J/Ψ signal and background contributions, which are also shown separately.

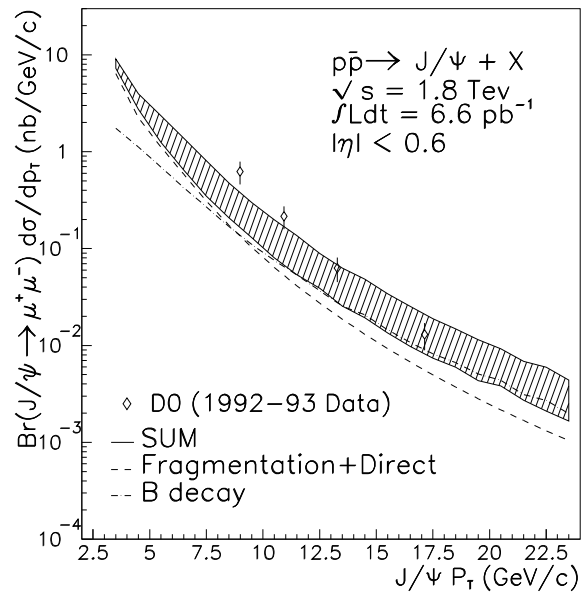


Figure 26: The product $B(d\sigma/dp_T)$ versus p_T for $J/\Psi \rightarrow \mu^+\mu^-$.

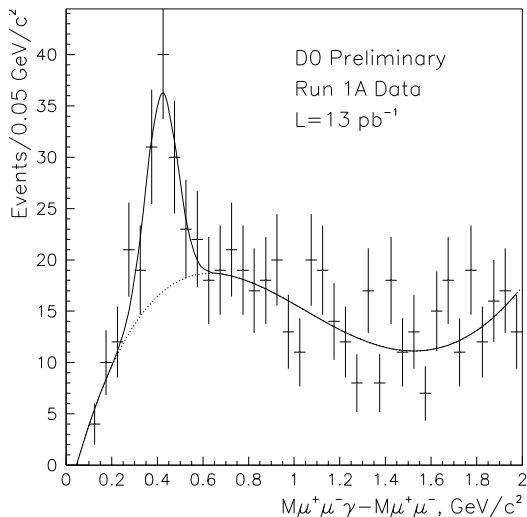


Figure 27: Mass difference $M(\mu\mu\gamma) - M(\mu\mu)$ for the $D\bar{0}\chi_c$ sample. This shows a clear signal for the decay $\chi_c \rightarrow \gamma J\Psi$.

9 Acknowledgement

This text is based on an internal $D\bar{0}$ note written by J. Hobbs with contributions from A. Brandt, H. Greenlee, W. Merritt, P. Quintas, and A. Zieminski. The results presented in this note have been updated using results presented at various conferences by W.Cobau, J. Ellison, B. Klima, L.Lueking, M. Paterno, S.Snyder, D.Zemienska. I would like to thank all these colleagues from $D\bar{0}$ for letting me use their material.

References

- [1] : “The $D\bar{0}$ Detector”, S. Abachi *et al.*, Nucl. Instr. and Meth. **338**, 185 (1994).
- [2] “First Generation Leptoquark Search in \bar{p} - p Collisions at $\sqrt{s} = 1.8$ TeV”, S. Abachi *et al.*, Phys. Rev. Letters **72**, 965 (1994). Limits given here are different from the published values because of an updated luminosity calculation using an average of E710 and CDF elastic cross sections
- [3] “Search for Squarks and Gluinos in \bar{p} - p Collisions at $\sqrt{s} = 1.8$ TeV”, S. Abachi *et al.*, Phys. Rev. Letters **75** 618, 1995.
- [4] “Search for the Top Quark in \bar{p} - p Collisions at $\sqrt{s} = 1.8$ TeV”, S. Abachi *et al.*, Phys. Rev. Letters **72**, 2138 (1994).
- [5] “Rapidity Gaps between Jets in \bar{p} - p Collisions at $\sqrt{s} = 1.8$ TeV”, S. Abachi *et al.*, Phys. Rev. Letters **72**, 2332 (1994).
- [6] “Search for High Mass Top Quark Production in \bar{p} - p Collisions at $\sqrt{s} = 1.8$ TeV”, S. Abachi *et al.*, Phys. Rev. Letters **74**, 2422 (1995).
- [7] “Observation of the Top Quark”, S. Abachi *et al.*, Phys Rev. Letters **74**, 2632 (1995).

- [8] “Inclusive μ and b -Quark Production Cross Sections in $p\bar{p}$ Collisions at $\sqrt{s} = 1.8$ TeV”, S. Abachi *et al.*, Phys. Rev. Letters **74**, 3548 (1995).
- [9] “Search for W Boson Pair Production in $\bar{p}p$ Collisions at $\sqrt{s} = 1.8$ TeV”, S. Abachi *et al.*, Phys. Rev. Letters **75**, 1023, 1995.
- [10] “Measurement of the $ZZ\gamma$ and $Z\gamma\gamma$ Couplings in $\bar{p}p$ Collisions at $\sqrt{s} = 1.8$ TeV”, S. Abachi *et al.*, Phys. Rev. Letters **75**, 1028, 1995.
- [11] “Measurement of the $WW\gamma$ Gauge Boson Coupling in $\bar{p}p$ Collisions at $\sqrt{s} = 1.8$ TeV”, S. Abachi *et al.*, Phys. Rev. Letters **75**, 1034, 1995.
- [12] “ W and Z Boson Production in $\bar{p}p$ Collisions at $\sqrt{s} = 1.8$ TeV”, S. Abachi *et al.*, Phys. Rev. Letters **75**, 1456 (1995).
- [13] “A Study of the Strong Coupling Constant Using $W +$ Jets Processes”, S. Abachi *et al.*, Phys. Rev. Letters, 75, 3226 (1995).
- [14] “Top Quark Search with the DØ 1992 – 93 Data Sample”, S. Abachi *et al.*, accepted for publication in Phys. Rev. **D** (Nov. 1, 1995).
- [15] “Transverse Energy Distributions within Jets in $\bar{p}p$ Collisions at 1.8 TeV”, S. Abachi *et al.*, Phys. Letters B357, 500 (1995).
- [16] “Search for Heavy W Bosons in 1.8 TeV $p\bar{p}$ Collisions”, S. Abachi *et al.*, Phys. Letters B358, 405 (1995).
- [17] “Second Generation Leptoquark Search in $\bar{p}p$ Collisions at 1.8 TeV”, S. Abachi *et al.*, accepted for publication in Phys. Rev. Letters.
- [18] “Studies of Topological Distributions of Inclusive Three- and Four-Jet Events in $p\bar{p}$ Collisions at $\sqrt{s} = 1800$ GeV with the DØ Detector”, S. Abachi *et al.*, submitted to Phys. Rev. D.
- [19] “Jet Production via Strongly-Interacting Color-Singlet Exchange in $\bar{p}p$ Collisions” S. Abachi *et al.*, submitted to Phys. Rev. Letters.
- [20] B. Klima (DØ Collaboration), FERMILAB-CONF-95/303-E. To be published in the Proceedings of the 17th International Symposium on Lepton-Photon Interactions, Beijing, China, Aug. 10-16, 1995.
- [21] D. Norman for the D0 Collaboration, Proceedings of the Meeting of the Division of Particles and Fields of the APS, Albuquerque, NM, 1994.
- [22] S. Abachi, et al., Fermilab PUB-95/057-E.
- [23] A. M. Jonckheere for the D0 Collaboration, Proceedings of Beyond the Standard Model IV, ed. J. Gunion, T. Han and J. Ohnemus, Dec 1994
- [24] S. Abachi *et al.*, Phys. Rev. Lett. **74** (1995) in press.

- [25] Dalitz and Goldstein Phys. Rev. **D45**, 1531
- [26] Kondo J. Phys. Soc. Japan **57**, 4126 and **60**, 836)
- [27] M. Mangano *et al.*, Nucl. Phys. **373**, 295 (1992).
- [28] CDF Collaboration, F. Abe *et al.*, Phys. Rev. Lett. **74**, 2626 (1995).
- [29] E. Laenen, J. Smith, and W. van Neerven, Phys. Lett. **321B**, 254 (1994).
- [30] D. Schaile, CERN-PPE/94-162, presented at 27th International Conference on High Energy Physics, Glasgow, July 1994 (unpublished).
- [31] CDF Collaboration, F. Abe *et al.*, Phys. Rev. D **50**, 2966 (1994); Phys. Rev. Lett. **73**, 225 (1994).
- [32] CDF Collaboration, F. Abe *et al.*, Phys. Rev. Lett. **69**, 3704 (1992).
- [33] F. Paige and S. Protopopescu, BNL Report no. BNL38034, 1986 (unpublished), release v6.49.
- [34] V. D. Barger and R. J. N. Phillips, *Collider Physics*, Addison-Wesley Publishing Co. (1987), p. 281.
- [35] F. A. Berends, H. Kuijf, B. Tausk, and W. T. Giele, Nucl. Phys. B357, 32 (1991).
- [36] F. Carminati *et al.*, "GEANT Users Guide," CERN Program Library, 1991 (unpublished).
- [37] G. Marchesini *et al.*, Comput. Phys. Commun. **67**, 465, (1992).
- [38] P. Nath and R. Arnowitt, Mod. Phys. Letters **A2**, 331 (1987).
- [39] "The ISASUSY Monte Carlo" by H. Baer and X. Tata. Now incorporated into the ISAJET Monte Carlo Beginning with v 7.0, by F. Paige, *et al.*
- [40] L. Sawyer, M. Sosebee, A. White, J White, "Search for $\tilde{W}_1 \tilde{Z}_2$ Production via Trilepton Final States", DØ Note 2520.
- [41] G.L. Kane, C. Kolda, L. Roszkowski, J.D. Wells, "The Constrained Minimal Supersymmetric Standard Model", UM-TH-93-24.
- [42] D. Norman, "A Search for a Second Generation Leptoquark", DØ Note 2290, April 14, 1995.
- [43] D. Norman, "Update on the Second Generation Leptoquark Analysis", DØ Note 2610, April 18, 1995.
- [44] A. Stange, W. Marciano, S. Willenbrock, "Higgs Bosons at the Fermilab Tevatron", Fermilab-Pub-93/142-T, BNL-49447.
- [45] A. Martin, R. Roberts, J.W. Stirling, Phys. Rev. D **47**, 867 (1993).
- [46] F. Boudjema *et al.*, Phys. Rev. D **43**, 2223 (1991)